Journal of Molecular Liquids 401 (2024) 124702

Contents lists available at ScienceDirect

Journal of Molecular Liquids

journal homepage: www.elsevier.com/locate/molliq

Protective action of water-soluble fullerene adducts on the example of an adduct with L-arginine

Vladimir V. Sharoyko [a,b,c,*], Olegi N. Kukaliia [a], Diana M. Darvish [d], Anatolii A. Meshcheriakov [a], Gleb O. Iurev [a,c,e], Pavel A. Andoskin [a], Anastasia V. Penkova [b], Sergei V. Ageev [a,b], Natalia V. Petukhova [a], Kirill V. Timoshchuk [a], Andrey V. Petrov [b], Aleksandr V. Akentev [b], Dmitry A. Nerukh [f], Anton S. Mazur [b], Dmitrii N. Maistrenko [c], Oleg E. Molchanov [c], Igor V. Murin [b], Konstantin N. Semenov [a,b,c,*]

[a] Pavlov First Saint Petersburg State Medical University, L'va Tolstogo str. 6–8, Saint Petersburg 197022, Russia
[b] Institute of Chemistry, Saint Petersburg State University, Universitetskii Pr. 26, Saint Petersburg 198504, Russia
[c] A. M. Granov Russian Research Centre for Radiology and Surgical Technologies, Leningradskaya Str. 70, Saint Petersburg 197758, Russia
[d] Institute of Cytology of the Russian Academy of Sciences, Tikhoretsky Pr. 4, Saint Petersburg, 194064, Russia
[e] Almazov National Medical Research Centre, Akkuratova Str., 2, Saint Petersburg 197341, Russia
[f] Aston University, Birmingham, B4 7ET, The United Kingdom

ARTICLE INFO

Keywords:
Fullerene
Collagen
Photoprotector
Radioprotector
Molecular Dynamics

ABSTRACT

We present radioprotective, antiglycating, and photoprotective properties of a water-soluble C_{60} fullerene derivative with L-arginine (C_{60}-Arg) and composite films based on collagen containing C_{60}-Arg. The synthesis of these materials is described. The identification of the synthesised materials was carried out using modern physicochemical methods of analysis. The physicochemical properties of aqueous solutions of C_{60}-Arg, such as, particle size distribution, zeta potentials, distribution coefficient in the octan-1-ol–water system were measured. The computer simulation of the process of C_{60}-Arg association in aqueous and isotonic solutions was carried out using Molecular Dynamics. Composite films based on collagen containing C_{60}-Arg demonstrate significant improvement in mechanical properties, cell adhesion, and cell proliferation when the nano-modifier is added. This shows high potential for the use of the C_{60}-Arg adduct in biomedicine.

1. Introduction

One of the most promising areas for the use of fullerenes and their derivatives is biology and medicine. This is due to the fact that fullerenes are highly reactive due to the presence of double bonds, they demonstrate high antioxidant activity, the ability to penetrate through the lipid bilayer, and modulate transmembrane ion transport [1–4].

Fullerene solubility is a serious problem, especially in connection with its potential applications in medicine. It is practically insoluble in an aqueous medium [5,6], due to its high hydrophobicity. However, approaches have been developed that allow the synthesis of water-soluble fullerene adducts with acceptable solubility of 10–200 mg•mL^{-1} for medical use [1–3,7].

Methods of synthesis of water-soluble fullerene adducts are currently in high demand, as the adducts have a wide range of biological activity: antioxidant [8], antimicrobial [9], membranotropic [10], antiviral [11,12], antitumour [13], neuroprotective [14,15], and photodynamic [16,17]. They can also act as radioprotectors, as well as inhibitors of enzymes and apoptosis (Fig. 1) [1–4,18,19]. Thus, fullerenes and its water-soluble adducts (fullerenols, carboxyfullerenes, adducts with amino acids) can serve as the basis for creating new high-tech medical materials and drugs. For example, it was shown [20,21] that fullerene adducts can sterically inhibit the HIV protease by incorporating into the active site cavity of the enzyme.

One of the most studied and promising classes of water-soluble fullerene adducts are adducts with amino acids and peptides [22–24]. The works [25–30] present approaches to the synthesis of these compounds; a fairly large number of publications are devoted to the thermodynamic properties of their solid phase, the physicochemical properties of solutions, and phase equilibria [30–34].

* Corresponding authors at: L'va Tolstogo Str. 6–8, Saint Petersburg, 197022, Russia.
E-mail addresses: sharoyko@gmail.com (V.V. Sharoyko), knsemenov@gmail.com (K.N. Semenov).

https://doi.org/10.1016/j.molliq.2024.124702
Received 13 August 2023; Received in revised form 29 February 2024; Accepted 7 April 2024
Available online 9 April 2024

Let us briefly describe the biomedical data on the adducts of light fullerenes with amino acids and peptides. In [35,36] the antiviral activity of C_{60} fullerene adducts with carnosine dipeptide, as well as sodium salts of aminobutyric and aminocaproic acids against cytomegalovirus infection (CMVI) was studied. It was found that the sodium salt of fullerenylaminobutyric acid inhibits the development of CMVI five times more effectively than ganciclovir. Khalikov *et al.* [37] studied the antiviral activity of the sodium salts of C_{60} fullerene adducts with amino acids against the H5N1 avian influenza virus on porcine embryonic kidney (PEKC) cell line in experiments *in vitro*. These compounds have been shown to be able to inhibit the replication of the H5N1 virus.

Bjelaković *et al.* [38] compared the antioxidant activity of *N*-substituted fulleropyrrolidines containing a peptide side chain using the FOX antioxidant assay. All compounds were shown to have a more pronounced antioxidant activity than vitamin C. Li *et al.* [27] studied the photodynamic properties of C_{60} fullerene adducts with L-phenylalanine and glycine on human hepatocarcinoma cell line (SMMC-7721) and found that these adducts can be used as photosensitisers for photodynamic therapy of tumour diseases. Hu *et al.* [28,39,40] studied the biological effect of C_{60} fullerene adducts with β-alanine, L-cystine, and glutathione on the rat adrenal medulla pheochromocytoma (PC12) cell line. The results of the study showed that fullerene adducts in the concentration range from 0.5 to 100 $\mu g \cdot mL^{-1}$ have an antiapoptotic effect on PC12 cells under the action of hydrogen peroxide. Hu *et al.* [41] studied the effect of C_{60} fullerene adducts with folacin and the amino acids β-alanine and L-valine on NO-induced apoptosis. The study showed that the fullerene adducts with amino acids block membrane lipid oxidation and mitochondrial membrane depolarisation, increase the activity of SOD, CAT, and GSH-Px enzymes, and thus prevent NO-mediated cell death by apoptosis. In the experiments *in vitro* and *in vivo*, the authors of [42] found that C_{60} fullerene adducts with various amino acids, L-phenylalanine, L-serine, β-alanine, and γ-phenylbutyric acid, inhibit the proliferation of glioblastoma cells and reduce the rate of their growth on the *Danio rerio* fish model. It was found that the adduct of fullerene C_{60} with L-phenylalanine inhibits the growth of glioblastoma without slowing down the recovery of neurons and without affecting neural stem cells. Jiang *et al.* [26] studied the biological effect of fullerene adduct with glycine on the cell lines of cervical cancer (HeLa) and mouse osteosarcoma (Lm8). As a result of the studies, it was found that the fullerene adduct with glycine upon irradiation (λ = 500–600 nm) causes dose-dependent death of the Lm8 cell line and induces apoptosis in the HeLa cell line. In [43], the biological effect of C_{60} fullerene adducts with folacin, L-phenylalanine, and L-arginine on HeLa tumour cells was studied. It was shown that when cells were irradiated with visible light, there was a decrease in the mitochondrial membrane potential, cell viability, activity of the enzyme superoxide dismutase, catalase and glutathione peroxidase, which ultimately lead to the activation of caspase-3 and the launch of the apoptosis program.

In [44] the membranotropic properties of C_{60}-Ala and C_{60}-Ala-Ala adducts were studied. These adducts have been shown to enter liposomes through the lipid bilayer of membranes. Also, the adducts of fullerenes with amino acids are able to carry out active transmembrane transport of Co^{2+} ions, forming complexes with it.

Thus, the pronounced potential for the use of adducts of light fullerenes with amino acids in biomedicine determines the importance of developing scalable methods for their production, as well as further studies of their physicochemical and biological properties. Another topical trend is the use of fullerene adducts as biopolymer nanomodifiers to obtain composite materials with unique properties. Such composite materials may include materials based on type I collagen, widely used in tissue engineering and regenerative medicine [45,46]. Collagen is able to have a haemostatic [47,48], wound healing [49], anti-inflammatory effects [50,51], and collagen-based materials have high biocompatibility and low immunogenicity. When developing biocomposites, collagen can play the role of a matrix that can hold a nanomodifier that

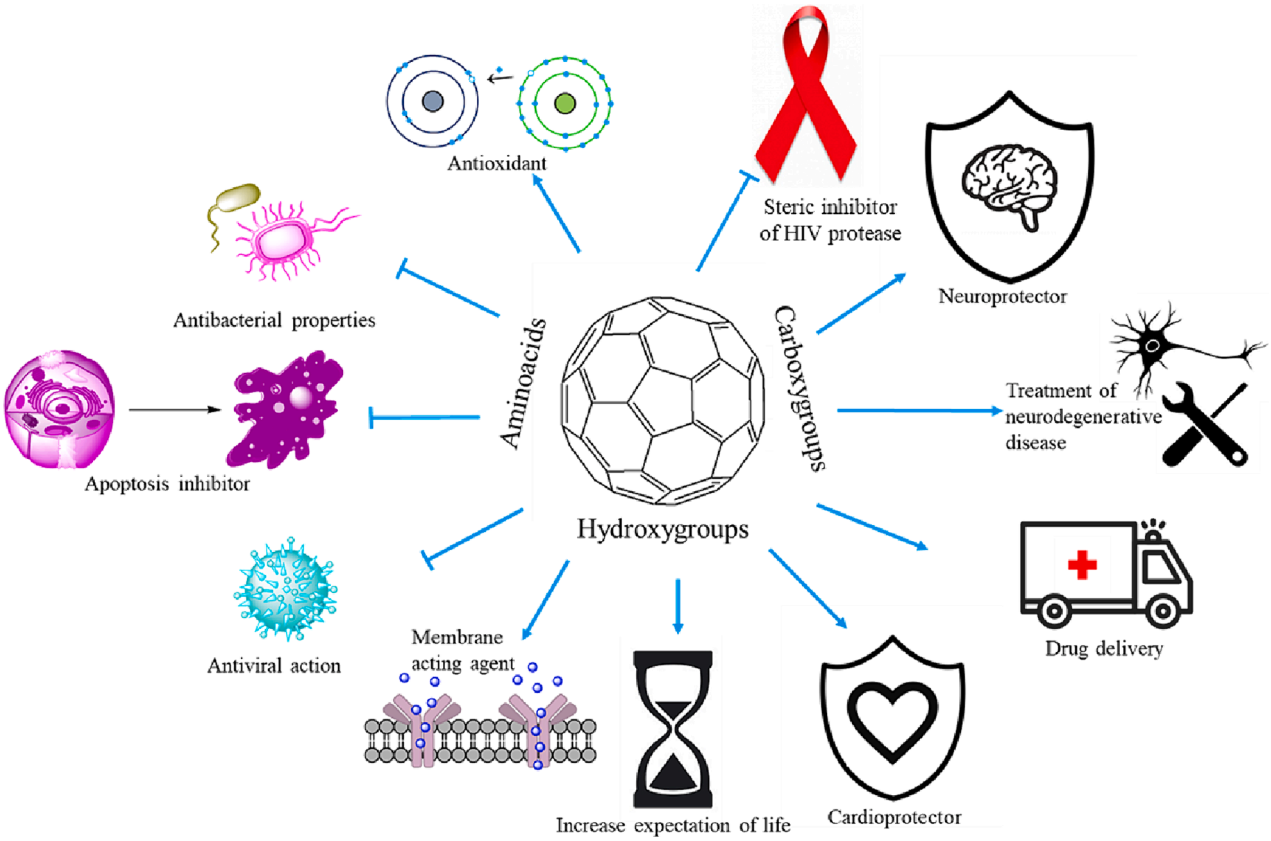

Fig. 1. Main biological properties of water-soluble fullerene adducts.

provide specific properties to the biocomposite. Such nanomodifiers can also be fullerene adducts with amino acids, which can improve the physicomechanical and biological properties of collagen.

This work is devoted to the study of the physicochemical and protective properties of C_{60}-Arg (radioprotective, photoprotective, antiglycation), as well as the synthesis and biological study of composite materials based on collagen.

2. Experimental part

2.1. Materials, synthesis and identification of the C_{60}-Arg adduct

The reagents used for the experiments are presented in Table S1. For the synthesis of the C_{60} fullerene adduct with L-arginine ($C_{60}(C_6H_{13}N_4O_2)_8H_8$, C_{60}-Arg, Fig. S1), C_{60} fullerene of 99.95 wt% grade purity, produced by ZAO MST Nano (St. Petersburg), L-arginine, sodium hydroxide, ethanol, toluene, and distilled water were used. The synthesis was carried out according to the method presented in [52].

The identification of C_{60}-Arg was carried out using a set of physicochemical methods, specifically: elemental analysis (Euro EA3028-HT), IR spectroscopy (Shimadzu FTIR-8400S spectrometer), solid-state ^{13}C NMR spectroscopy (Bruker Advance III 400 WB; operating frequency 100.64 MHz for ^{13}C), electron spectroscopy (SHIMADZU UV-2600i), HPLC (Shimadzu LC-20 Prominence) and thermogravimetric analysis (NETZSCH TG 209 F1 Libra).

2.2. Physicochemical study of C_{60}-Arg solutions

The distribution of C_{60}-Arg in octan-1-ol–H_2O system was studied using a LAUDA ET 20 thermostatic shaker (shaking frequency 80 Hz). The temperature was maintained within 0.1 K, the experiment time was 5 h. To carry out the experiment, a solution of C_{60}-Arg ($C = 0.01$ g·dm^{-3}) in deionised water was prepared, to which an equal volume of octan-1-ol (5 mL) was added. After reaching equilibrium, an aliquot of the aqueous phase was taken. The distribution coefficient of C_{60}-Arg was calculated according to the following equation:

$$P_{ow} = \frac{c_o^{'}}{c_w^{'}} = \frac{c_w - c_o^{'}}{c_w^{'}} \quad (1)$$

where $c_o^{'}$ and $c_w^{'}$ are C_{60}-Arg concentrations in organic and aqueous phases, respectively, c_w is the initial concentration of C_{60}-Arg in water.

The concentration of C_{60}-Arg in the aqueous phase was determined by spectrophotometric method ($l = 1$ cm) at the wavelength of $\lambda = 330$ nm according to Eq. (2):

$$C = 0.095 \cdot A_{330} \quad (2)$$

where C is the concentration of C_{60}-Arg, A_{330} is the optical density of the solution at $\lambda = 330$ nm.

Fig. S2 of the Supplementary Material shows the electronic spectra of C_{60}-Arg aqueous solutions, as well as individual C_{60} in *o*-xylene (for comparison) and the concentration dependence of the optical density at $\lambda = 330$ nm, demonstrating the fulfilment of the Bouguer–Beer–Lambert law.

The concentration dependences of the size distribution of C_{60}-Arg associates and the ζ-potential in aqueous solutions in the concentration range $C = 0.001$–10 g·dm^{-3} were obtained using Malvern Zetasizer 3000 (Great Britain) instrument at $T = 298.15$ K.

2.3. Investigation of C_{60}-Arg solutions at the atomic-molecular level

To study the nature of the C_{60}-Arg association at the atomic-molecular level, the methods of computational quantum chemistry and molecular dynamics were used. The electronic structure of C_{60}-Arg was computed by DFT in accordance with the scheme that we previously used in [53] applying PBE functional and atomic basis DNP v. 4.4 with full geometry optimisation and taking into account the interaction with the solvent (water) according to COSMO model. For DFT calculations the DMol^3 module from Materials Studio 7.0 program package was used. The charge density isosurface of Saturn-like isomer in the COSMO model is shown in Fig. S3. The choice of functional and basis set was based on numerous successful applications of this scheme to predict NMR spectra, thermodynamic parameters and structural properties of fullerene adducts [54–56]. Molecular Dynamics was used to study the evolution of the interaction of C_{60}-Arg adducts with each other in aqueous medium, as well as in physiological solution (0.15 M NaCl). The charges on the atoms, estimated according to the Mulliken scheme, were used from quantum chemical calculations. For Molecular Dynamics, GROMACS 2022 package was used. For calculations with periodic boundary conditions, 20 C_{60}-Arg molecules and approximately $1.3{\cdot}10^5$ water molecules were placed in a cubic box with 16 nm sides; the distance between C_{60}-Arg molecules was at least 30 Å, the distance from the C_{60}-Arg molecule to the wall was at least 15 Å; the diameter of the C_{60}-Arg molecule was 20–25 Å. The force field for the OPLS-AA/M system was used for calculations; the simulation time was 200 ns with a step of 1 fs; the initial arrangement of molecules in the cell is shown in Fig. 2a,b. The initial configurations for modelling the association process were created using the PACKMOL package. Further, in the GROMACS 2022 package, the system solvation, energy minimization, and equilibration were performed in NVT and NPT ensembles with Berendsen thermostat and barostat for 400 ps with the time step of 0.1 fs under the condition $T = 298.15$ K, $P = 1$ bar.

2.4. Synthesis, identification, and properties of composite materials based on C_{60}-Arg and collagen

Type I collagen was extracted by acid solubilisation from rat tail tendons. Rat tail tendons were dissolved in 0.5 M acetic acid and precipitated twice, first with 0.9 M NaCl and then with 0.02 M Na_2HPO_4. The precipitate was again dissolved in 0.5 M acetic acid, after which it was purified by dialysis against the same acid with a gradual decrease in its concentration. As a result, collagen solution with the concentration of 5 mg•mL^{-1} in 0.1 % acetic acid was obtained.

To prepare collagen gels containing C_{60}-Arg (Fig. S4), solutions of C_{60}-Arg were preliminarily prepared with the concentrations of 1.25, 2.5, 5, and 10 mg•mL^{-1}, then collagen was mixed with neutralising saline and C_{60}-Arg solution in the 9:1:1 vol ratio. 500 μL of each gel sample was taken, thus, the concentration of C_{60}-Arg in the film samples was $C = 0.125$, 0.25, 0.5, and 1.0 mg·mL^{-1}. Collagen films were obtained by drying collagen gels. To study the mechanical properties of collagen films, the gels were cast into rectangular moulds 40 × 10 mm in size and then dried in an oven at 30 °C.

The identification of collagen and composite materials was carried out using several physicochemical methods: IR spectroscopy (Shimadzu FTIR-8400S spectrometer), solid-state ^{13}C NMR spectroscopy (Bruker Advance III 400 WB; operating frequency 100.64 MHz for ^{13}C), thermogravimetric analysis (NETZSCH TG 209 F1 Libra) and atomic force spectroscopy (NT-MDT Spectrum Instruments, Moscow, Russia).

The mechanical properties of collagen films were studied using Instron 1122 universal setup (Great Britain) in the active loading mode at a constant strain rate of 10 mm·min^{-1}.

The contact angles were measured by the sessile drop method using LK-1 Goniometer (OOO NPK Open Science, Krasnogorsk, Russia). The results obtained were processed using DropShape program.

To study cell adhesion, the wells of the plate were coated with collagen or collagen modified with C_{60}-Arg. Then, cells of the HEK293 line were seeded into the plates and incubated in the plates for 2 h. Wells with standard surface treatment (SPL Life Sciences Co Ltd.) were used as controls. At the end of the incubation, non-adherent cells were carefully removed by washing with phosphate-buffered saline (PBS), and the number of adherent cells was counted using a Burker chamber.

Cell proliferation was assessed using sulphorodamine B. HEK293

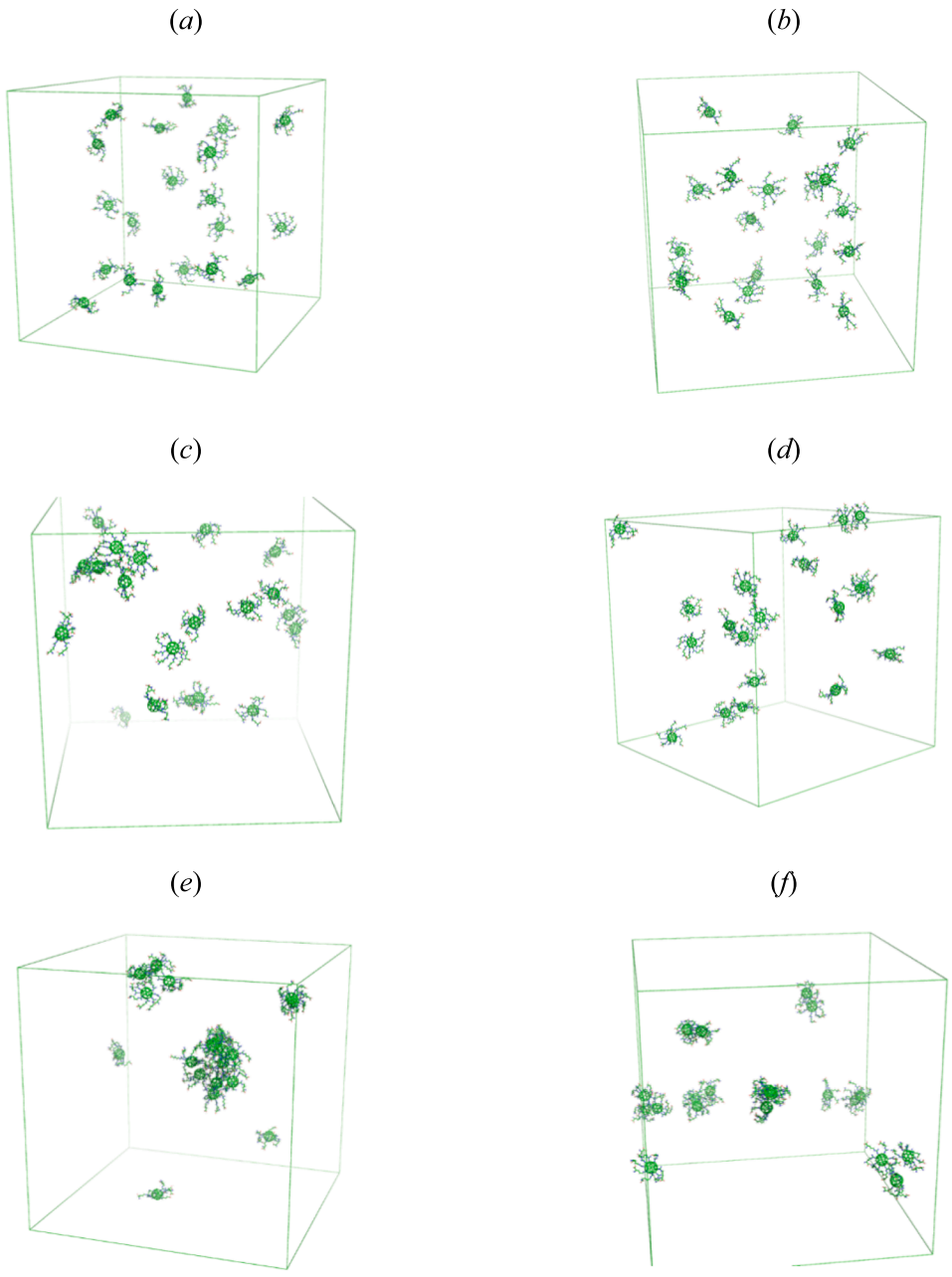

Fig. 2. Molecular dynamics visualisation for C60-Arg: initial arrangement of C60-Arg molecules in a cell without water molecules (a) and in saline (b); association of C60-Arg molecules in water after 10 ns (c) and in saline after 5 ns (d); formation of a large stable cluster consisting of C60-Arg molecules in saline after 50 ns (e); association of C60-Arg molecules after 100 ns in water (f) and in saline (g); association of C60-Arg molecules after 200 ns in water (h) and in saline (i).

cells were seeded in a 96-well microplate at the concentration of $2{\cdot}10^4$ cells per well. Cells were incubated for 48 h in wells whose surface was coated with collagen or collagen modified with C_{60}-Arg or without collagen coating (control), then 100 μL of 10 wt% trichloroacetic acid. The plates were incubated at 4 °C for 1 h, washed with distilled water, and dried at room temperature. After adding 100 μL of 0.057 wt% the solution of sulphorodamine B in 1 wt% acetic acid plates were incubated at room temperature for 30 min and washed four times with 1 wt% acetic acid to remove unbound dye. Optical density measurements were carried out at 510 nm using Allsheng AMR-100 plate reader (China) after adding 200 μL of 10 mM Tris buffer solution (pH 10.5; Paneco, Russia) to each well.

2.5. Protective effects

2.5.1. Radioprotective effect of C_{60}-Arg

Laboratory white rats of the *Wistar* line (males) weighing 300–350 g were used. The animals were obtained from the Rappolovo nursery, Leningrad oblast. The rats were kept at the vivarium of A.M. Granov Russian Research Centre for Radiology and Surgical Technologies in accordance with accepted sanitary standards (normal light and temperature conditions (20–22 °C), free access to water, nutritionally balanced granular feed (LBK-120 of the Tosnensky feed mill)) in standard cages with wood shavings bedding. All experimental work was carried out in compliance with the international recommendations of the European Convention for the Protection of Vertebrate Animals Used for Experimental and other Scientific Purposes (ETS 123), Strasbourg,

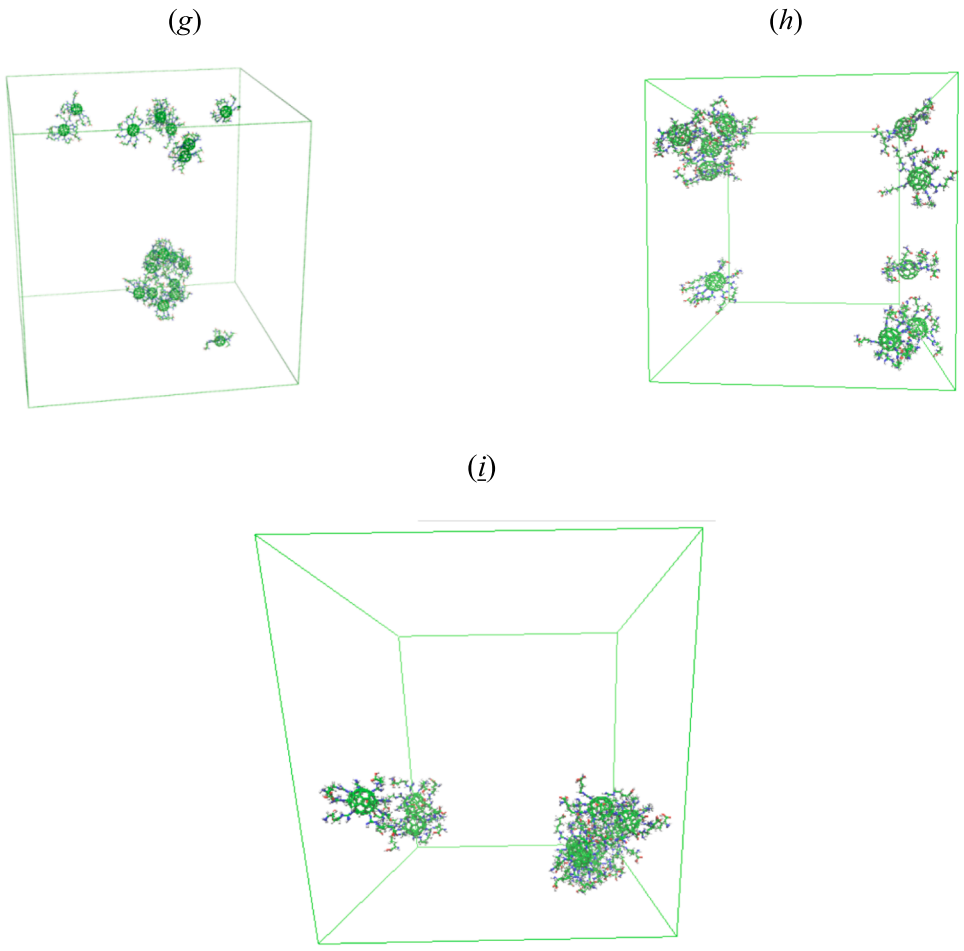

Fig. 2. (*continued*).

1986.

For experiments, four groups of 40 rats were formed from weight randomised animals: an intact control group (1), an irradiation group (2), a group of animals that received C_{60}-Arg (*3*), and the group of animals that received C_{60}-Arg and irradiated (*4*). Animals were previously kept in quarantine for 12 days. Clinical parameters (hair condition, food excitability, urination, coordination of movements) were assessed by visual assessment. Groups 3 and 4 received C_{60}-Arg once intraperitoneally at the dose of 2.5 mL per animal (8 mg·kg^{-1}). Then, 2.5–3 h after injection, Group 4 was subjected to general irradiation with γ-rays on a linear accelerator Elekta Synergy (Sweden) with the total dose of 8 Gy. Group (2) was irradiated in a similar way. Subsequently, all groups were kept under the same conditions as before the study. Animals were observed daily for the next 30 days. The survival rate of rats was determined, the general condition of the animals was recorded, attention was paid to the condition of the mucous membranes of the nose, skin and coat, behavioural features and the level of physical activity, the presence of anxiety, excitability, dysfunction of the gastrointestinal tract.

2.5.2. Antiglycation properties

The effect of C_{60}-Arg on HSA glycation was studied *in vitro* by changing the specific fluorescence of advanced glycation end products (AGEs) at λ_{ex} = 370 nm, $\lambda_{max/em}$ = 440 nm. Control samples (samples with glycation without C_{60}-Arg) contained 0.5 mL HSA (C = 0.06 mM), 0.4 mL glucose solution (C = 0.4 M) in PBS (pH 7.4), and 0.1 mL PBS (pH 7.4). Experimental samples (samples with glycation in the presence of C_{60}-Arg) contained 0.5 mL of HSA (C = 0.06 mM), 0.4 mL of glucose solution (C = 0.4 M) in PBS (pH 7.4), and 0.1 mL of C_{60}-Arg solution (C = 1, 10, 25, 50, 75, 100 μM) in PBS (pH 7.4). Reference samples (without glucose) contained 0.5 mL HSA (C = 4 mg•mL^{-1}), 0.4 mL phosphate buffer solution (pH 7.4), and 0.1 mL C_{60}-Arg in PBS (pH 7.4) (C = 1, 10, 25, 50, 75, 100 μM). All samples were incubated in a thermostat for 48 h at 60 °C. The reaction was stopped by adding 0.02 mL of trichloroacetic acid (50 wt%) to all samples; after 10 min, the samples were centrifuged for 15 min at 14,500 rpm at 6 °C. The supernatant was removed from the tubes, and the precipitate was redissolved in 1 mL of PBS (pH 10) by adding NaOH solution (C = 0.25 M). The specific fluorescence intensity of glycated HSA was measured on Solar CM2203 spectrofluorimeter (Republic of Belarus).

2.5.3. Photoprotective effect

Collagen solutions (3 mg·mL^{-1}) in the absence and presence of C_{60}-Arg (C = 0.5, 1, 5, and 10 μM) were irradiated at room temperature in quartz cuvettes in a UVC-3 ultraviolet camera (power 25 W, wavelength 254 nm, State Ryazan Instrument Plant, Russian Federation), the exposure time was from 0 to 20 min with the step of 5 min. Emission registration was carried out at the wavelength of 320 nm with the excitation wavelength of 290 nm.

3. Results and discussion

3.1. Identification of the C_{60}-Arg adduct

To establish the composition of C_{60}-Arg, elemental analysis was carried out, the results of which are consistent with theoretical calculations, experimental C 61.35 %, H 5.37 %, N 21.20 %, theoretical C 61.35 %, H 5.34 %, N 21.20 %.

Fig. 3 shows the ^{13}C NMR spectrum of C_{60}-Arg, which has the following bands: *a* is the band of carbon in the carboxyl group (176.9 ppm), *b* is the band of carbon in the guanidine group (158.8 ppm), *c* is the band of α-carbon atom in L-arginine (55.6 ppm); *d*, *e* are the bands of carbon atoms in $–CH_2–$ groups (42.3, 27.8 ppm), as well as the bands of carbon atoms in the fullerene core (139.3, 75.6, 63.8, 16.5 ppm). The spectral line with a chemical shift of 75.6 ppm can be attributed to carbon of the fullerene core bonded to the hydrogen atom.

The IR spectrum of a solid C_{60}-Arg sample in a KBr pellet (Fig. S5) includes the following peaks (cm^{-1}): 3430 — νO–H, 2900 — νC–H, 1605 — νC = O, 1390 — νC–N, 1140 — (νN–C_{60}), 515 — (C_{60} core).

Fig. S2a shows the electronic absorption spectra of the aqueous solution of C_{60}-Arg and C_{60} in *o*-xylene. The following conclusions can be drawn from the obtained spectra: (*i*) the electronic spectrum of the aqueous solution of C_{60}-Arg does not contain absorption bands; (*ii*) in the spectrum of the aqueous solution of C_{60}-Arg there is no absorption peak characteristic to fullerene C_{60} ($\lambda = 335$ nm); (*iii*) the comparison of the spectra of C_{60}-Arg and C_{60} solutions confirms the fullerene functionalisation and the absence of unreacted C_{60} fullerene.

The purity of C_{60}-Arg was determined by HPLC with UV detection at 300 nm, using the Phenomenex® NH2 column (150 mm × 2.0 mm, 5 μm, 100 Å), the injection volume was $2{\cdot}10^{-8}$•m^3, the injection rate was 0.2 mL·min^{-1}, the eluent was acetonitrile / 0.1 % aqueous solution of acetic acid (5 / 95). Based on the chromatographic data, the purity of the C_{60}-Arg derivative was determined to be 99.8 % (Fig. S6).

Fig. S7 shows the results of thermogravimetric analysis of C_{60}-Arg. The obtained data demonstrate the following: (*i*) in the temperature range up to 340 K, the C_{60}-Arg adduct is thermally stable; (*ii*) in the temperature range $T = 340–950$ K, multistage decomposition processes of C_{60}-Arg (in the presence of O_2) occur, including dehydration, decarboxylation, denitrogenation, and dehydrogenation; the weight loss of 65.9 % corresponds to the degradation of eight L-arginine residues; (*iii*) in the temperature range $T = 950–1270$ K, the fullerene core is oxidised.

3.2. Physicochemical study of C_{60}-Arg solutions

The main factor determining the ability of a biologically active compound to penetrate the target and become distributed throughout the body is lipophilicity. A lgP_{ow} value between − 1 and + 2 is considered to be optimal for substances intended for oral administration. At a low value of lgP_{ow}, the compound will be poorly absorbed and, as a result, have low bioavailability. With a high value of lgP_{ow}, the compound will be completely retained in the lipid layers. The increase in lipophilicity correlates with the increase in biological activity, the decrease in water solubility, the acceleration of metabolism and slowing excretion. Also, high lipophilicity makes it easy to penetrate the skin (transdermal application) [57]. The value of the logarithm of the C_{60}-Arg distribution coefficient was $lgP_{ow} = 0.23$. This value shows that C_{60}-Arg has almost the same affinity for the aqueous and lipid phases.

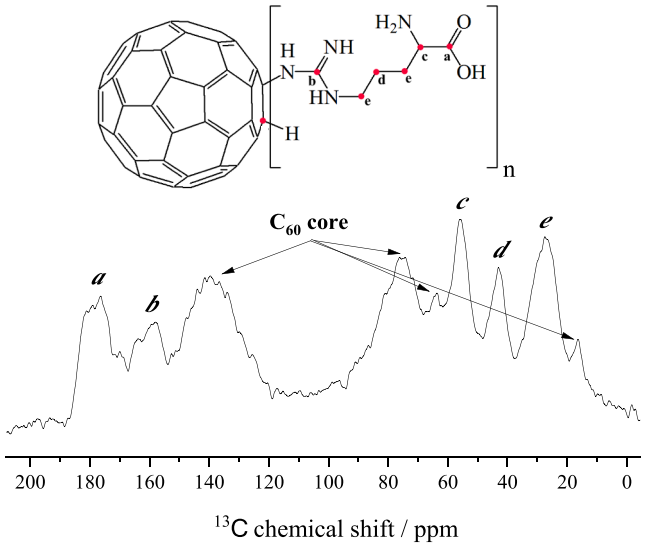

Fig. 3. 13C NMR spectrum of C60-Arg.

The analysis of the concentration dependences of C_{60}-Arg associates size distribution and ζ-potentials in aqueous solutions in the concentration range $C = 0.001–10$ g•dm^{-3} at $T = 298.15$ K (Fig. S8) shows the following: (*i*) the absence of monomeric C_{60}-Arg molecules with linear dimensions of 2 nm over the entire range of concentrations; (*ii*) the presence of associates of the first and second types in the concentration range $C = 0.001–0.1$ g•dm^{-3} with linear dimensions of 50–70 nm and 200–300 nm, respectively; (*iii*) the presence associates of the second type only in the concentration range $C = 0.1–0.2$ g•dm^{-3}; (*iv*) the simultaneous presence of associates of the second and third orders (5–6 μm) in the solution in the concentration range $C = 0.3–10$ g dm^{-3}. The analysis of the concentration dependence of the ζ-potential shows that: (*i*) in the entire range of concentrations, the values of the ζ-potential are negative and equal to −(60–20) mV; (*ii*) in the studied concentration range, C_{60}-Arg solutions are aggregately stable; (*iii*) the distribution of the ζ-potential includes two peaks related to the associates of the first and second types in the concentration range $C = 0.001–0.1$ g•dm^{-3}; one peak related to the associates of the second type in the concentration range $C = 0.2–5$ g•dm^{-3}; two peaks related to the associates of the second and third types in the concentration range $C = 5–10$ g•dm^{-3}; (*iv*) the comparison of experimental data shows a discrepancy between the dimensions of the associates in the concentration range $C = 0.1–3$ g•dm^{-3}. Most likely, this is due to the fact that, under the action of an electric potential, charged C_{60}-Arg particles can associate or dissociate, depending on the ratio of the surface charges and the degree of cluster hydration.

To study the state of C_{60}-Arg in aqueous medium, its electronic structure, total energy, and binding energy were calculated in the form of a neutral molecule and in the form of zwitterion. The calculation was carried out using DMol^3 program, where DFT method is implemented; in water environment and using the COSMO model. For calculations, the PBE functional and the DNP v. 4.4 basis were used. The transfer of proton to amino group attached to the α-carbon atom of L-arginine residue increased the binding energy to −50.481 Ha (for the comparison, the binding energy of C_{60}-Arg in neutral state is equal to −50.568 Ha).

Calculated energy of HOMO level is −169976 and LUMO level is −0.126207 Ha in C_{60}-Arg molecule. The visualisation of these orbitals are in Fig. 4a,b. The calculations of the electronic structure showed that the electron density is concentrated both on the carbons of the fullerene core and on the oxygen and nitrogen atoms of amino acid residues (Fig. 4c). At the same time, the carbon atoms of the fullerene core, connected to amino acid residues, donate their electrons to the nearest nitrogen atom. Thus, the interaction of C_{60}-Arg molecules with each other can occur both through atoms with an increased electron density of the fullerene core, and through the amino acid residues. To further elucidate the possible ways of C_{60}-Arg aggregation, Molecular Dynamics was used. In modelling the association of C_{60}-Arg molecules in physiological saline, it was found that the approach of C_{60}-Arg nanoparticles to each other occurred quite dynamically, by 5 ns the dimers of C_{60}-Arg molecules were formed in the system (Fig. 2d), while in water the dimer formation occurs by 10 ns (Fig. 2c). Further, by 50 ns, a large associate formed in physiological saline, consisting of 10 C_{60}-Arg molecules 6–7 nm in size, which persisted until the end of the calculations (Fig. 2e). At the end of the simulation in physiological saline, the remaining 10 C_{60}-Arg molecules were either combined into small groups of up to three C_{60}-Arg molecules, or remained as individual molecules. In contrast to the simulation in physiological saline, more uniform association of C_{60}-Arg molecules was observed in water with the formation of groups consisting of two or three molecules. Large size associates were formed

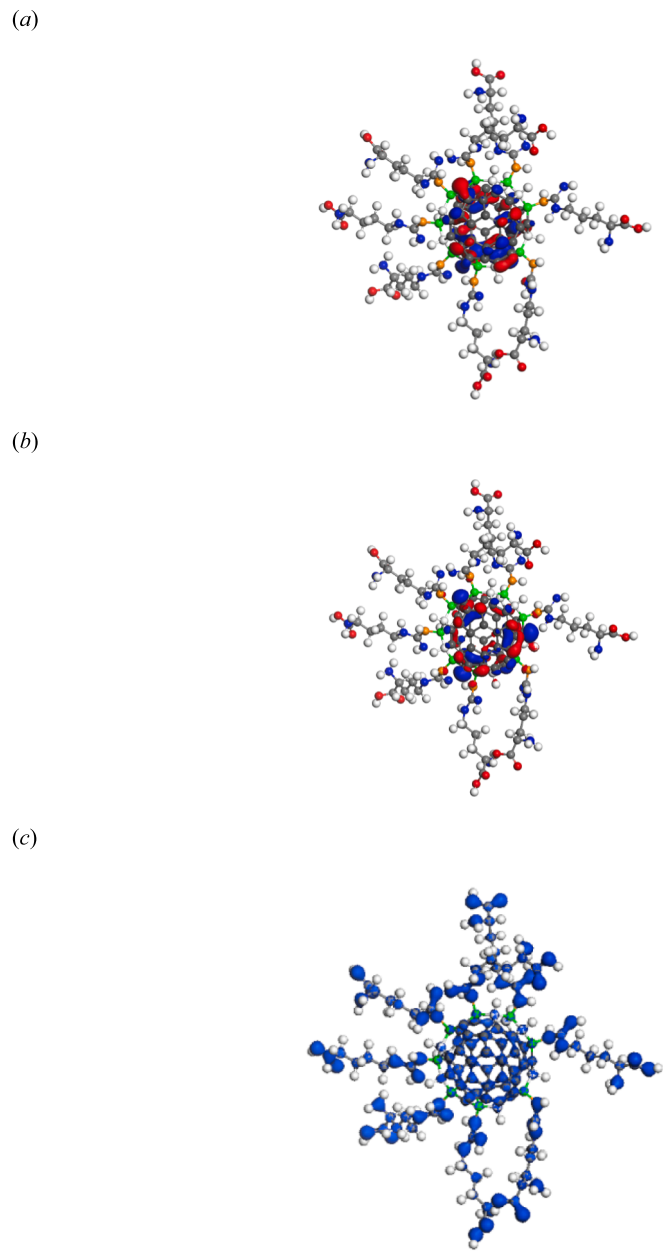

Fig. 4. HOMO visualisation (a), LUMO visualisation (b), total electron density map (c).

for a short time during the simulation. Fig. 2f–*i* shows the arrangement of C_{60}-Arg molecules after 100 ns and 200 ns in water and saline. The higher potential for clustering in saline is further evidenced by the reduction in solvent-accessible surface during the simulation compared to the behaviour of C_{60}-Arg molecules in water (Fig. 5).

3.3. Protective properties of C_{60}-Arg

3.3.1. Radioprotective properties of C_{60}-Arg

The results of studying the radioprotective properties of C_{60}-Arg are shown in Table 1. One day after irradiation in Groups 2 and 4 at the dose of 8 Gy, the following clinical manifestations of radiation sickness were observed in animals: inhibited motor activity, depression, ruffled coat. Visible mucous membranes were pale. Later, there was a disorder in the function of the gastrointestinal tract (diarrhoea) and brown discharge from the nasal passages and eyes.

Death in Group (2) (control) was 100 % on the 11th day after the experiment. In the group of animals after irradiation and treated with C_{60}-Arg (Group 4), the death of animals was 75 %. In the remaining Groups (1) and (3), the death of animals was not observed.

3.3.2. Antiglycating properties of C_{60}-Arg

As a result of the experiment on HSA glycation in the presence of C_{60}-Arg, with increase in the concentration of the latter, more intense inhibition of the formation of glycated HSA occurs. This is the reason for the decrease in the concentration of formed AGEs in the sample, which leads to the decrease in the intensity of the detected fluorescence signal compared to the fluorescence of glycated HSA without C_{60}-Arg. Fig. 6 shows the dependence of the intensity of HSA glycation on the concentration of C_{60}-Arg. Thus, we show that C_{60}-Arg exhibits antiglycation activity *in vitro*. The calculated IC_{50} value for C_{60}-Arg was 45 μM.

3.3.3. Photoprotective properties

Fig. 7 shows the results before and after the exposure to UV light of aqueous collagen solutions in the absence and presence of C_{60}-Arg. It can be seen that as the irradiation time increases, the fluorescence intensity decreases. This is due to two effects: photocrosslinking and photodegradation of collagen. Photocrosslinking causes the conformational transition of the collagen molecule (helix-coil), which leads to the decrease in emission due to shielding of tryptophan residues. Photodegradation leads to the decrease in collagen concentration, which is accompanied by the change in the fluorescence spectrum. Both of these effects are associated in the literature with the formation of reactive oxygen species during UV irradiation. Therefore, substances exhibiting antiradical activity can also exhibit photoprotective properties [58]. To assess the protective effect of the C_{60}-Arg adduct in UV-induced collagen damage, we calculated the changes in the fluorescence intensity before and after irradiation ($F_d = (F_0 - F_t) / F_0$), which characterise the relative changes in fluorescence due to photocrosslinking and photodegradation of collagen. The dependence of F_d on t showed that the exposure of collagen to UV radiation in the presence of the C_{60}-Arg derivative leads to the dose-dependent decrease in collagen photodegradation and photocrosslinking. The Scatchard equation was used to determine the binding constant (K_b) and the number of binding sites (n) of C_{60}-Arg to collagen:

$$\lg\frac{F_0 - F}{F} = \lg K_b + n\lg Q \tag{3}$$

where F_0 and F are fluorescence intensities in the absence and presence of the quencher, Q is the quencher concentration. From the dependence in Hill coordinates $\lg[(F_0 - F) / F]$ on $\lg Q$ (Fig. S9), the following values were obtained: $K_b = (1.08 \pm 0.03)\cdot 10^7$ M^{-1} and $n = 1.39 \pm 0.04$. The obtained value of the binding constant indicates that C_{60}-Arg forms a strong complex with RatCol, and thus provides a photoprotective effect. Therefore, the C_{60}-Arg adduct has a potential for developing photoprotective nanomaterials.

3.4. Identification and study of the properties of composite materials based on C_{60}-Arg and collagen

Fig. S10 and 11 show the IR spectra of collagen, C_{60}-Arg, and composite films based on collagen containing C_{60}-Arg at various concentrations. The spectrum of pure collagen (Fig. S11) shows the presence of characteristic bands: at 3300 cm^{-1} — νN–H, νO–H (amide I), 1540 cm^{-1} — νC–N and δC–H (amide II), 1650 cm^{-1} — νC = O in peptides, 1240 cm^{-1} — νC–C (amide III), which is consistent with the literature data [59]. The spectra of the composite films show a shift in the maxima of the absorption bands corresponding to the stretching vibrations of C = O in the region of 1650 cm^{-1}, as well as N–H and O–H in the region of 3300 cm^{-1}, compared with the spectrum of individual C_{60}-Arg. This fact is associated with the formation of hydrogen bonds between the groups having an electron-deficient hydrogen atom and the groups having an

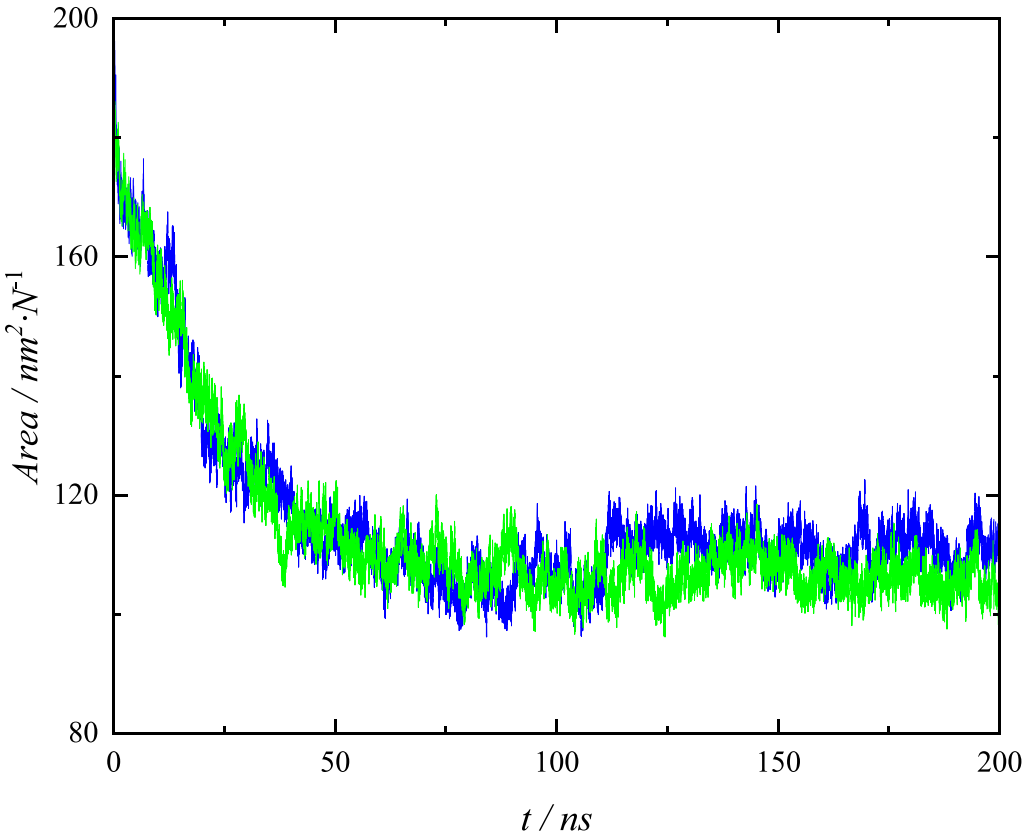

Fig. 5. Change in the surface area of C60-Arg molecules available to the solvent during molecular dynamics in water (shown in blue) and in saline (shown in green).

Table 1
Scheme of the experiment on the radioprotective effect.

Animal group number	Number of rats in the group	Name of the substance	Method of substance administration	Dose / mL	Radiation dose / Gy	Animal death
1	10	—	—	—	—	no
2	10	—	—	—	8	11th day — death is 100 %
3	10	C_{60}-Arg	intraperitoneally	2.5	—	no
4	10	C_{60}-Arg	intraperitoneally	2.5	8	11th day — death is 75 %

atom with high electronegativity.

Fig. 8 shows the ^{13}C NMR spectrum of collagen, which has peaks corresponding to the carbon atoms of the amino acids that make up collagen: 17.4 ppm — β carbon atom of L-alanine (Ala β); 27.8 ppm — β carbon atom of L-proline (Pro β); 42.8 ppm — α carbon atom of glycine (Gly α); 50.2 ppm — δ carbon atom of L-proline (Pro δ); 60.4 ppm — α carbon atom of L-proline (Pro α), α carbon atom of L-hydroxyproline (Hyp α), δ carbon atom of L-hydroxyproline (Hyp δ); 70.5 ppm — γ carbon atom of L-hydroxyproline (Hyp γ); the signal at 173.3 ppm corresponds to the carbon atom of the carbonyl group (C = O). The resulting spectrum is consistent with the literature data [60–62].

Fig. 9 shows the ^{13}C NMR spectra of collagen films with different contents of C_{60}-Arg. The comparison of the spectra shows that the band corresponding to the γ-carbon atom of L-proline at 50.2 ppm is weak in the spectra of the composite films. This effect may be due to hydrophobic interactions between the non-functionalised regions of the fullerene core and the non-polar part of the pyrrolidine ring of L-proline. It was previously noted that in the most stable C_{60}-Arg isomer, amino acid residues are not evenly distributed on the fullerene core, but are localized in the equatorial region of the molecule; moreover, they do not have a zwitterionic structure. Taking into account the electronic structure of C_{60}-Arg, one can also assume the formation of hydrogen bonds between the nitrogen atoms of the imino group, which have an unshared electron pair, as well as hydroxyl, amino, and carboxyl groups of amino acids that make up collagen. However, the complex nature of the spectra does not allow to detect changes associated with the formation of hydrogen bonds.

Fig. S12 shows the results of thermogravimetric analysis of collagen and collagen films containing C_{60}-Arg at various concentrations. From Fig. S12, it can be seen that the *TG* curves of collagen and collagen films containing C_{60}-Arg have two areas of weight loss. In the temperature range up to 100 °C, the dehydration of collagen films occurs (mass loss is about 10 %). In the temperature range of 225–500 °C, processes associated with the thermal decomposition of collagen films most likely occur (mass loss is 50–60 % for all samples). The obtained experimental data indicate that the introduction of C_{60}-Arg into the composition of collagen films leads to a dose-dependent increase in thermal stability. This effect may be associated with the structuring action of C_{60}-Arg due to the formation of the network of hydrogen bonds and hydrophobic interactions.

Fig. 10 shows an example of the AFM photograph of a collagen film containing 0.125 mg·mL^{-1} C_{60}-Arg. The analysis of this image shows that under the described experimental conditions, a film is formed that contains C_{60}-Arg associates up to 20 nm in size. At the same time, it is

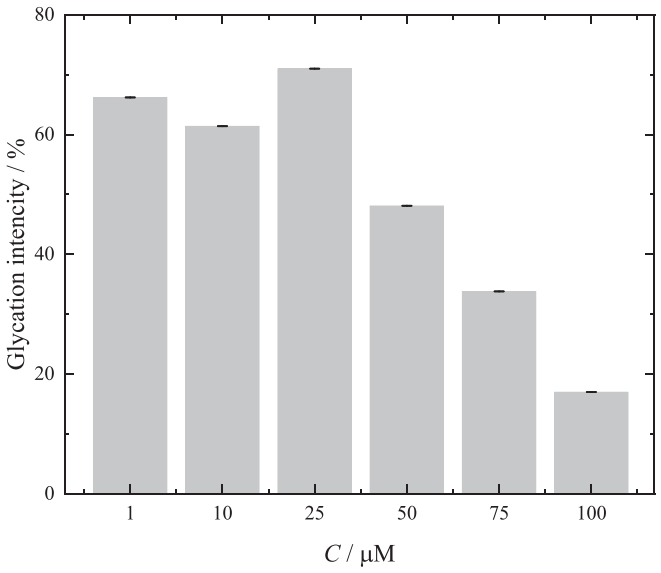

Fig. 6. Concentration dependence of HSA glycation inhibition in the presence of C60-Arg at various concentrations. C is the molar concentration of C60-Arg.

clear that the nanoparticles are evenly distributed in the composite material. Table 2 shows the AFM images, mean (S_a), and root mean square (S_q) surface roughness of the collagen samples and collagen films modified with C_{60}-Arg. It can be seen that the increase in the content of C_{60}-Arg in the collagen film leads to the dose-dependent effect of increasing the surface roughness. The data obtained are consistent with the literature, where it was previously described that the use of carbon nanostructures (fullerenes, carbon nanotubes, graphenes) as a dopant for collagen films led to an increase in surface roughness [63–67]. It was shown in [68] that the increase in roughness leads to the increase in cell adhesion and proliferation. Thus, the obtained collagen films containing C_{60}-Arg can be considered as promising materials for biomedical applications.

The contact angles of wetting of composite materials showed (Fig. S13) that the addition of C_{60}-Arg as a modifier leads to decrease in the value of the contact angle, and, consequently, to increase in the hydrophilicity of the surface.

The mechanical properties of composite films showed (Fig. S14 and

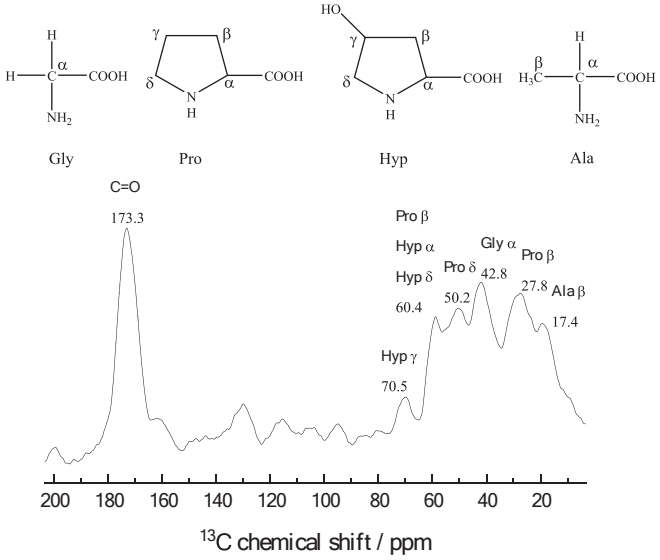

Fig. 8. ^{13}C NMR spectrum of collagen.

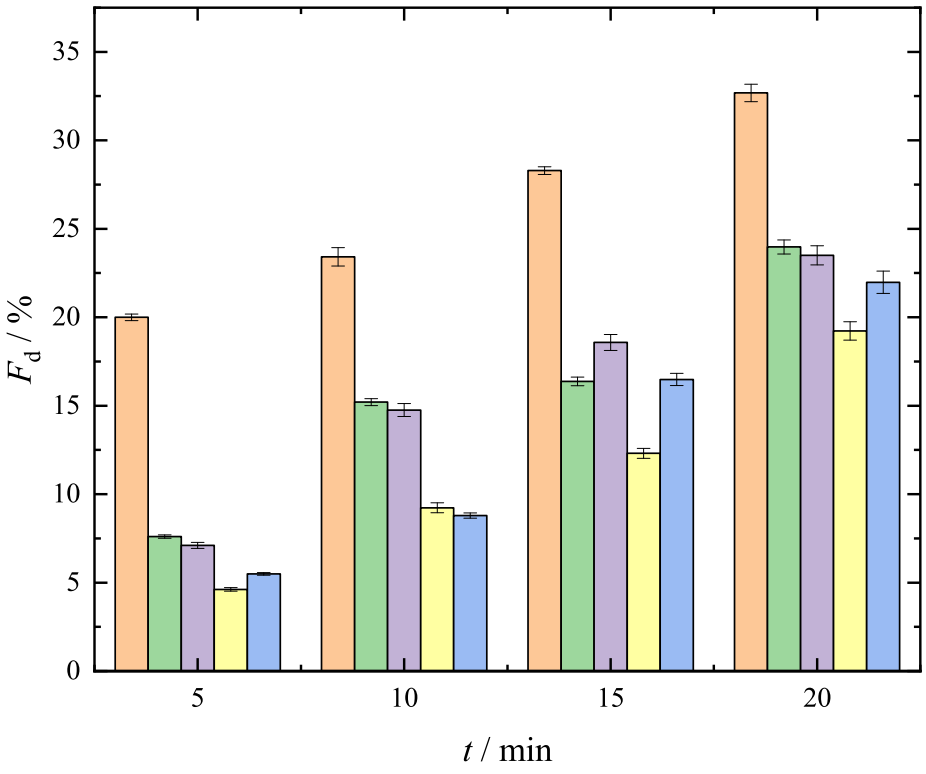

Fig. 7. Relative changes in collagen fluorescence under UV irradiation in the absence and presence of C60-Arg at various concentrations: C = 0 (—), 0.5 (—), 1.0 (—), 5.0 (—), 10.0 (—) μM.

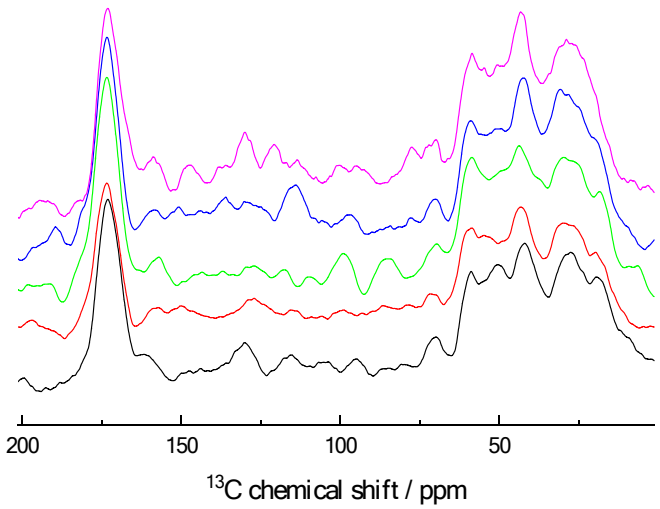

Fig. 9. 13C NMR spectra of collagen (—) and collagen films with different content of C60-Arg: C = 0 (black), 0.125 (red), 0.25 (green), 0.5 (blue), 1.0 (violet) mg·mL^{-1}.

(*a*)

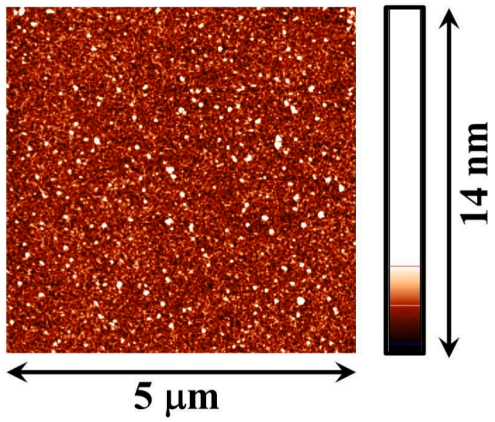

(*b*)

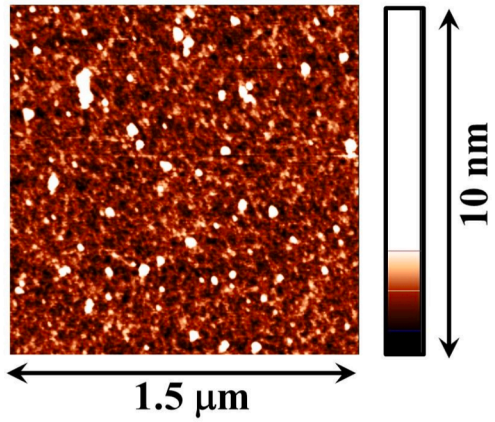

Fig. 10. AFM images of collagen films containing C60-Arg (C = 0.125 mg·mL^{-1}).

Table S2) that the introduction of C_{60}-Arg leads to significant change in mechanical properties. Films with high content of C_{60}-Arg had the breaking tension and the elongation at break two times more than unfilled collagen films. The results obtained also indicate the increase in the number of intermolecular bonds in the film structure in the presence of C_{60}-Arg. Visually, the change in the mechanical properties of collagen films can be assessed by interaction with water: a drop of water flowing down the film caused pure collagen film to roll up, while the films modified with C_{60}-Arg remained straightened (Fig. S15). Obviously, the described intermolecular interactions will significantly affect the physicomechanical properties of collagen films. Previously, our group investigated aqueous solutions of fullerene adducts and showed that the addition of nanoparticles leads to compaction and structuring of the solution, as evidenced by the significant absolute value and negative sign of the partial molar volumes of fullerene adducts [30–34]. The influence of carbon nanoparticles on the physicochemical and mechanical characteristics of various materials is widely described in literature [1–4]. Using cement-containing systems as an example, our group described the following scheme of nanoparticle action: water-soluble fullerene adducts structure water (which can be seen from the values of partial molar volumes of the fullerene derivative), then the fullerene adduct structures the aqueous solution involved in hardening the polymerising material, and, finally, the polymerising material inherits its structure [69]. In [70], Molecular Dynamics was used to study aqueous solutions containing collagen and nanomodifiers, among which fullerenol ($C_{60}(OH)_{24}$) and endohedral fullerenol with an encapsulated gadolinium atom ($Gd@C_{82}(OH)_{22}$) were considered. It was shown that these nanoparticles contribute to the formation of fibrils, which leads to increased rigidity of the native structure, due to the formation of a network of additional hydrogen bonds. The degree of impact of fullerene adducts depends on its surface charge and the presence of hydrophilic groups in the structure.

Fig. 11 shows data on the adhesion of HEK293 cells to composite collagen films containing C_{60}-Arg. From the obtained results, it can be seen that the cell adhesion increases with the increase in the content of C_{60}-Arg in composite films.

Fig. 12 shows data on the effect of composite collagen films containing C_{60}-Arg on the proliferation of HEK293 cell line. As can be seen from Fig. 12, the proliferation of HEK293 cells on collagen films increases with the increase in the content of C_{60}-Arg, and at C = 1.0 mg·mL^{-1} it was 200 % compared to the control.

The data obtained demonstrate the promise of using the synthesised composites in regenerative medicine, combustiology, and tissue engineering.

4. Conclusions

The synthesis and identification of C_{60}-Arg was carried out and for the first time solid-state ^{13}C NMR spectroscopy was used to characterise the adduct. The physicochemical properties of aqueous solutions of C_{60}-Arg showed that the solutions are strongly associated, and in the concentration range C = 0.001–10 g dm^{-3} the aggregates were of 5–6 μm in size. The presence of associates in aqueous solution was also confirmed by Molecular Dynamics modelling. The calculated distribution coefficient in the octan-1-ol–water system was $\lg P_{ow}$ = 0.23, which indicates the amphiphilicity of C_{60}-Arg. The protective properties of C_{60}-Arg demonstrate that this material has potential in developing radioprotectors, antiglycating agents, and photoprotectors. It was found that the mortality of rats treated with C_{60}-Arg at the concentration of 8 mg·kg^{-1} after irradiation with γ-rays at the total dose of 8 Gy decreased by 25 % compared with the control group. The inhibition of HSA glycation in the presence of C_{60}-Arg (C = 100 μM) was more than 80 %. The introduction of C_{60}-Arg nanoparticles into collagen leads to a dose-dependent decrease in photodegradation by 1.5–2 times.

Composite films with different contents of C_{60}-Arg (C = 0.125–1.0 mg·mL^{-1}) were also synthesised. The introduction of a nanomodifier (C = 1.0 mg·mL^{-1}) leads to significant improvement in the mechanical properties, namely, a twofold increase in the breaking stress and elongation at break; a 6-fold increase in cell adhesion (C = 1.0 mg·mL^{-1}), as

Table 2
AFM images, average (S_a) and root mean square (S_q) surface roughness of collagen samples and collagen films containing C_{60}-Arg, C = 0.125, 0.25, 0.5, 1.0 mg·mL^{-1}.

C / mg·mL^{-1}	3D AFM image	AFM image	Surface roughness parameters, nm
0	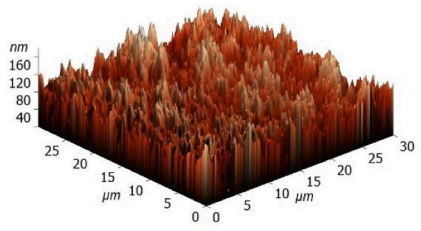	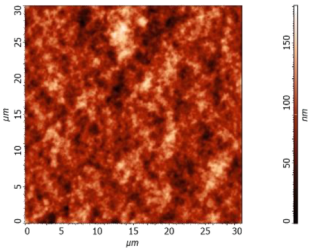	S_a = 17.7374 S_q = 22.3547
0.125	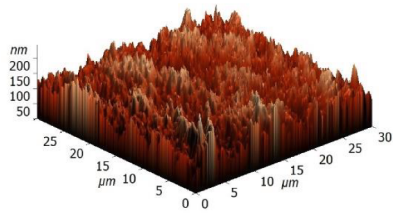	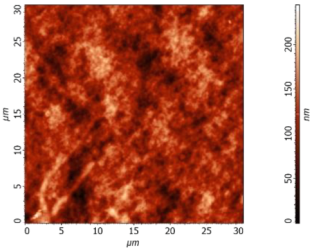	S_a = 22.9045 S_q = 28.953
0.25	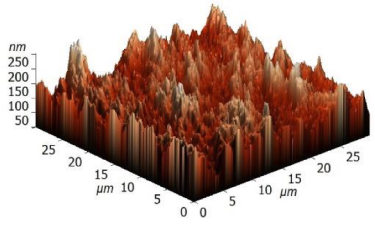	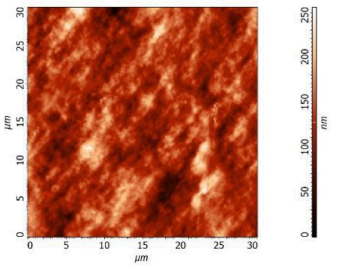	S_a = 24.9903 S_q = 31.5824
0.5	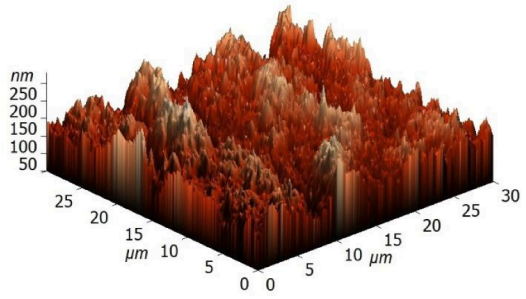	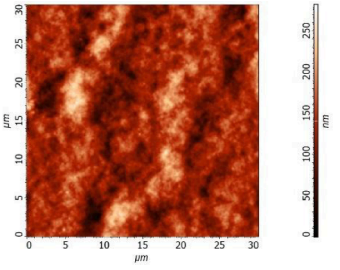	S_a = 28.1417 S_q = 36.082
1.0	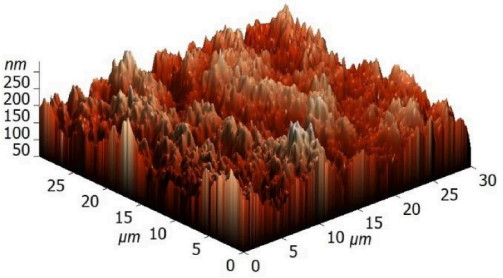	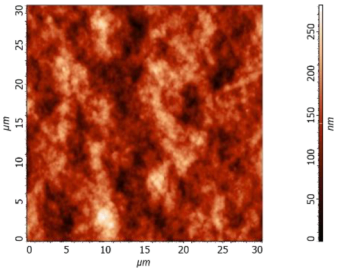	S_a = 30.3581 S_q = 37.7579

well as increase in cell proliferation by 200 % (C = 1.0 mg·mL^{-1}) compared to unmodified collagen. The obtained results demonstrate significant potential in using water-soluble fullerene adducts in biomedicine.

CRediT authorship contribution statement

Vladimir V. Sharoyko: Resources, Investigation, Funding acquisition. **Olegi N. Kukaliia:** Investigation. **Diana M. Darvish:** Investigation. **Anatolii A. Meshcheriakov:** Methodology, Funding acquisition. **Gleb O. Iurev:** Investigation. **Pavel A. Andoskin:** Investigation. **Anastasia V. Penkova:** Resources, Investigation. **Sergei V. Ageev:** Writing – review & editing, Writing – original draft, Visualization, Data curation. **Natalia V. Petukhova:** Software, Investigation. **Kirill V. Timoshchuk:** Investigation, Software. **Andrey V. Petrov:** Software, Investigation. **Aleksandr V. Akentev:** Writing – review & editing, Investigation. **Dmitry A. Nerukh:** Writing – review & editing, Writing – original draft, Software, Investigation. **Anton S. Mazur:**

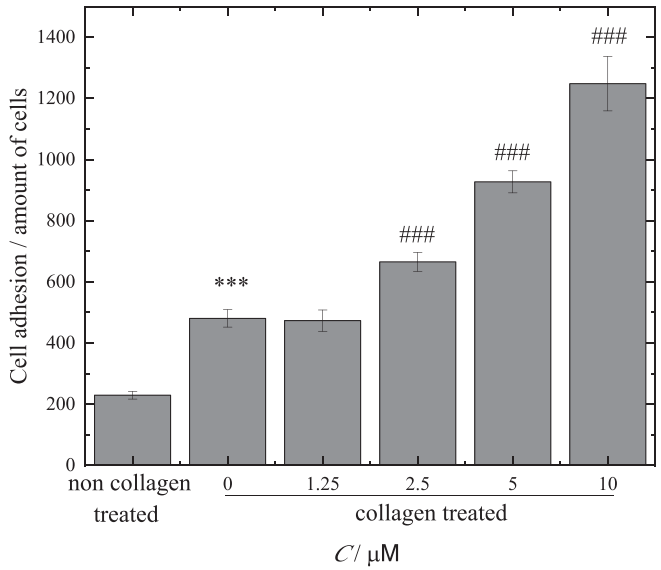

Fig. 11. Influence of collagen and collagen films with different content of C60-Arg on the adhesion of HEK293 cells. Data are presented as mean ± standard error of the mean. ***p < 0.001 compared to wells uncoated with collagen; ###p < 0.001 compared to wells coated with C60-Arg-free collagen.

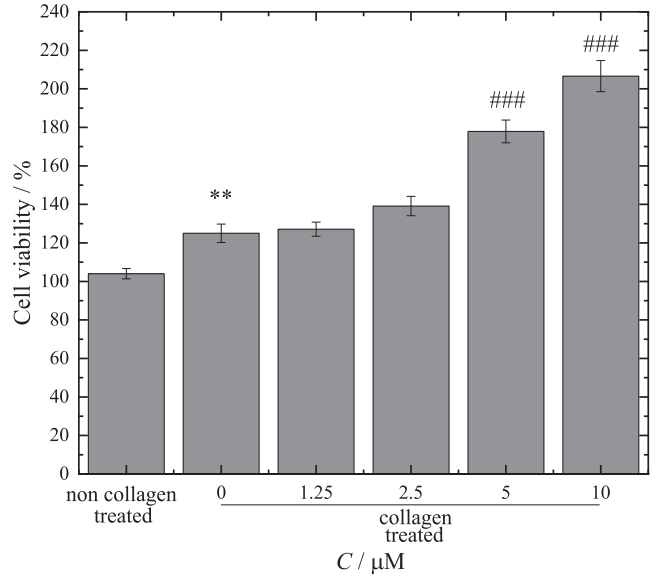

Fig. 12. Influence of collagen and collagen films with different content of C60-Arg on the proliferation of HEK293 cells. Data are presented as mean ± standard error of the mean. **p < 0.01 compared to wells without collagen; ###p < 0.001 compared to wells coated with collagen and not containing C60-Arg.

Investigation. **Dmitrii N. Maistrenko:** Resources, Investigation. **Oleg E. Molchanov:** Resources, Investigation. **Igor V. Murin:** Funding acquisition, Conceptualization. **Konstantin N. Semenov:** Validation, Supervision, Project administration, Formal analysis, Conceptualization.

Declaration of competing interest

The authors declare that they have no known competing financial interests or personal relationships that could have appeared to influence the work reported in this paper.

Data availability

Data will be made available on request.

Acknowledgments

The work was carried out with the financial support of the Ministry of Health of the Russian Federation 'Development of a radioprotector based on water-soluble forms of nanocarbon modified with l-amino acids' EGISU: 123020800170-8. The equipment of the following Resource Centres of the Research Park of Saint Petersburg State University was used: Computing Centre, the Centre for Diagnostics of Functional Materials for Medicine, Pharmacology and Nanoelectronics, Magnetic Resonance Research Centre, Centre for Chemical Analysis and Materials Research, Thermogravimetric and Calorimetric Research. D. N. acknowledges the use of HPC Midlands+supercomputer funded by EPSRC, grant number EP/P020232/1; the access to Sulis Tier 2 HPC platform hosted by the Scientific Computing Research Technology Platform at the University of Warwick. Sulis is funded by EPSRC Grant EP/T022108/1 and the HPC Midlands+consortium. The collaboration was supported by the program H2020-MSCA-RISE-2018, project AMR-TB, Grant ID: 823922.

Appendix A. Supplementary material

Supplementary material to this article can be found online at https://doi.org/10.1016/j.molliq.2024.124702.

References

[1] K.N. Semenov, N.A. Charykov, V.N. Postnov, V.V. Sharoyko, I.V. Vorotyntsev, M. M. Galagudza, I.V. Murin, Fullerenols: physicochemical properties and applications, Prog. Solid State Chem. 44 (2016) 59–74, https://doi.org/10.1016/j.progsolidstchem.2016.04.002.

[2] K.N. Semenov, E.V. Andrusenko, N.A. Charykov, E.V. Litasova, G.G. Panova, A. V. Penkova, I.V. Murin, L.B. Piotrovskiy, Carboxylated fullerenes: physico-chemical properties and potential applications, Prog. Solid State Chem. 47–48 (2017) 19–36, https://doi.org/10.1016/j.progsolidstchem.2017.09.001.

[3] E.I. Pochkaeva, N.E. Podolsky, D.N. Zakusilo, A.V. Petrov, N.A. Charykov, T. D. Vlasov, A.V. Penkova, L.V. Vasina, I.V. Murin, V.V. Sharoyko, K.N. Semenov, Fullerene derivatives with amino acids, peptides and proteins: from synthesis to biomedical application, Prog. Solid State Chem. 57 (2020) 100255, https://doi.org/10.1016/j.progsolidstchem.2019.100255.

[4] V.V. Sharoyko, S.V. Ageev, N.E. Podolsky, A.V. Petrov, E.V. Litasova, T.D. Vlasov, L.V. Vasina, I.V. Murin, L.B. Piotrovskiy, K.N. Semenov, Biologically active water-soluble fullerene adducts: das glasperlenspiel (by H. Hesse)? J. Mol. Liq. 323 (2021) 114990 https://doi.org/10.1016/j.molliq.2020.114990.

[5] V.N. Bezmel'nitsyn, A.V. Eletskii, M.V. Okun, Fullerenes in solutions, Phys. Usp. 41 (1998) 1091–1114, https://doi.org/10.1070/PU1998v041n11ABEH000502.

[6] D. Bagchi, M. Bagchi, H. Moriyama, F. Shahidi, Bio-Nanotechnology, Blackwell Publishing Ltd., Oxford, UK, 2013. 10.1002/9781118451915.

[7] K. Matsubayashi, K. Kokubo, H. Tategaki, S. Kawahama, T. Oshima, One-step synthesis of water-soluble fullerenols Bearing nitrogen-containing substituents, Fullerenes, Nanotubes, Carbon Nanostruct. 17 (2009) 440–456, https://doi.org/10.1080/01490450903039263.

[8] I.C. Wang, L.A. Tai, D.D. Lee, P.P. Kanakamma, C.-K.-F. Shen, T.-Y. Luh, C. H. Cheng, K.C. Hwang, C_{60} and water-soluble fullerene derivatives as antioxidants against radical-initiated lipid peroxidation, J. Med. Chem. 42 (1999) 4614–4620, https://doi.org/10.1021/jm990144s.

[9] N. Tsao, T.-Y. Luh, C.-K. Chou, J.-J. Wu, Y.-S. Lin, H.-Y. Lei, Inhibition of group a streptococcus infection by carboxyfullerene, Antimicrob. Agents Chemother. 45 (2001) 1788–1793, https://doi.org/10.1128/aac.45.6.1788-1793.2001.

[10] I.M. Andreev, V.S. Romanova, A.O. Petrukhina, S.M. Andreev, Amino-acid derivatives of fullerene C_{60} behave as lipophilic ions penetrating through biomembranes, Phys. Solid State 44 (2002) 683–685, https://doi.org/10.1134/1.1470559.

[11] M.G. Medzhidova, M.V. Abdullaeva, N.E. Fedorova, V.S. Romanova, A.A. Kushch, *In vitro* antiviral activity of fullerene amino acid derivatives in cytomegalovirus infection, Antibiot. Khimioter. 49 (2004) 13–20.

[12] Y.-L. Lin, H.-Y. Lei, Y.-Y. Wen, T.-Y. Luh, C.-K. Chou, H.-S. Liu, Light-independent inactivation of dengue-2 virus by carboxyfullerene C_3 Isomer, Virology 275 (2000) 258–262, https://doi.org/10.1006/viro.2000.0490.

[13] X.L. Yang, C.H. Fan, H.S. Zhu, Photo-induced cytotoxicity of malonic acid [C60] fullerene derivatives and its mechanism, Toxicol. In Vitro 16 (2002) 41–46, https://doi.org/10.1016/S0887-2333(01)00102-3.

[14] L.L. Dugan, D.M. Turetsky, C. Du, D. Lobner, M. Wheeler, C.R. Almli, C.K.F. Shen, T.-Y. Luh, D.W. Choi, T.-S. Lin, Carboxyfullerenes as neuroprotective agents, Proc. Natl. Acad. Sci. 94 (1997) 9434–9439, https://doi.org/10.1073/pnas.94.17.9434.

[15] L.L. Dugan, E.G. Lovett, K.L. Quick, J. Lotharius, T.T. Lin, K.L. O'Malley, Fullerene-based antioxidants and neurodegenerative disorders, Parkinsonism Relat Disord. 7 (2001) 243–246, https://doi.org/10.1016/S1353-8020(00)00064-X.

[16] F. Käsermann, C. Kempf, Buckminsterfullerene and photodynamic inactivation of viruses, Rev. Med. Virol. 8 (1998) 143–151, https://doi.org/10.1002/(SICI)1099-1654(199807/09)8:3<143::AID-RMV214>3.0.CO;2-B.

[17] B. Vileno, A. Sienkiewicz, M. Lekka, A.J. Kulik, L. Forró, *In vitro* assay of singlet oxygen generation in the presence of water-soluble derivatives of C_{60}, Carbon N Y. 42 (2004) 1195–1198, https://doi.org/10.1016/j.carbon.2003.12.042.

[18] S. Trajković, S. Dobrić, V. Jaćević, V. Dragojević-Simić, Z. Milovanović, A. Đorđević, Tissue-protective effects of fullerenol $C_{60}(OH)_{24}$ and amifostine in irradiated rats, Colloids Surf. B Biointerfaces. 58 (2007) 39–43, https://doi.org/10.1016/j.colsurfb.2007.01.005.

[19] J. Grebowski, P. Kazmierska, G. Litwinienko, A. Lankoff, M. Wolszczak, A. Krokosz, Fullerenol $C_{60}(OH)_{36}$ protects human erythrocyte membrane against high-energy electrons, biochimica et biophysica acta (BBA) -, Biomembranes 1860 (2018) 1528–1536, https://doi.org/10.1016/j.bbamem.2018.05.005.

[20] S.H. Friedman, D.L. DeCamp, R.P. Sijbesma, G. Srdanov, F. Wudl, G.L. Kenyon, Inhibition of the HIV-1 protease by fullerene derivatives: model building studies and experimental verification, J. Am. Chem. Soc. 115 (1993) 6506–6509, https://doi.org/10.1021/ja00068a005.

[21] S.H. Friedman, P.S. Ganapathi, Y. Rubin, G.L. Kenyon, Optimizing the binding of fullerene inhibitors of the HIV-1 Protease through predicted increases in hydrophobic desolvation, J. Med. Chem. 41 (1998) 2424–2429, https://doi.org/10.1021/jm970689r.

[22] A. Bianco, T. Da Ros, M. Prato, C. Toniolo, Fullerene-based amino acids and peptides, J. Pept. Sci. 7 (2001) 208–219, https://doi.org/10.1002/psc.313.

[23] A. Krokosz, Fullerenes in biology, Rostok, Saint Petersburg, 2007.

[24] G.A. Burley, P.A. Keller, S.G. Pyne, [60]Fullerene amino acids and related derivatives, Fuller. Sci. Technol. 7 (1999) 973–1001, https://doi.org/10.1080/10641229909350301.

[25] V.S. Romanova, V.A. Tsyryapkin, Y.I. Lyakhovetsky, Z.N. Parnes, M.E. Vol'pin, Addition of amino acids and dipeptides to fullerene C_{60} giving rise to monoadducts, Russ. Chem. Bull. 43 (1994) 1090–1091, https://doi.org/10.1007/BF01558092.

[26] G. Jiang, F. Yin, J. Duan, G. Li, Synthesis and properties of novel water-soluble fullerene–glycine derivatives as new materials for cancer therapy, J. Mater. Sci. Mater. Med. 26 (2015) 24, https://doi.org/10.1007/s10856-014-5348-4.

[27] Z. Li, L.-L. Pan, F.-L. Zhang, Z. Wang, Y.-Y. Shen, Z.-Z. Zhang, Preparation and characterization of fullerene (C60) amino acid Nanoparticles for liver cancer cell treatment, J. Nanosci. Nanotechnol. 14 (2014) 4513–4518, https://doi.org/10.1166/jnn.2014.8242.

[28] Z. Hu, W. Guan, W. Wang, L. Huang, H. Xing, Z. Zhu, Synthesis of β-alanine C_{60} derivative and its protective effect on hydrogen peroxide-induced apoptosis in rat pheochromocytoma cells, Cell Biol. Int. 31 (2007) 798–804, https://doi.org/10.1016/j.cellbi.2007.01.013.

[29] A.A. Shestopalova, K.N. Semenov, N.A. Charykov, V.N. Postnov, N.M. Ivanova, V. V. Sharoyko, V.A. Keskinov, D.G. Letenko, V.A. Nikitin, V.V. Klepikov, I.V. Murin, Physico-chemical properties of the C_{60}-arginine water solutions, J. Mol. Liq. 211 (2015) 301–307, https://doi.org/10.1016/j.molliq.2015.07.022.

[30] K.N. Semenov, N.A. Charykov, G.O. Iurev, N.M. Ivanova, V.A. Keskinov, D. G. Letenko, V.N. Postnov, V.V. Sharoyko, N.A. Kulenova, I.V. Prikhodko, I. V. Murin, Physico-chemical properties of the C60-l-lysine water solutions, J. Mol. Liq. 225 (2017) 767–777, https://doi.org/10.1016/j.molliq.2016.11.003.

[31] V.V. Sharoyko, S.V. Ageev, A.A. Meshcheriakov, N.E. Podolsky, J.P. Vallejo, L. Lugo, I.T. Rakipov, A.V. Petrov, A.V. Ivanova, N.A. Charykov, K.N. Semenov, Physicochemical investigation of water-soluble $C_{60}(C_2NH_4O_2)_4H_4$ (C60-Gly) adduct, J. Mol. Liq. 344 (2021) 117658, https://doi.org/10.1016/j.molliq.2021.117658.

[32] A.A. Meshcheriakov, G.O. Iurev, M.D. Luttsev, N.E. Podolsky, S.V. Ageev, A. V. Petrov, L.V. Vasina, I.L. Solovtsova, V.V. Sharoyko, I.V. Murin, K.N. Semenov, Physicochemical properties, biological activity and biocompatibility of water-soluble C_{60}-Hyp adduct, Colloids Surf. B Biointerfaces. 196 (2020) 111338, https://doi.org/10.1016/j.colsurfb.2020.111338.

[33] V.V. Sharoyko, S.V. Ageev, A.A. Meshcheriakov, A.V. Akentiev, B.A. Noskov, I. T. Rakipov, N.A. Charykov, N.A. Kulenova, B.K. Shaimardanova, N.E. Podolsky, K. N. Semenov, Physicochemical study of water-soluble $C_{60}(OH)_{24}$ fullerenol, J. Mol. Liq. 311 (2020) 113360, https://doi.org/10.1016/j.molliq.2020.113360.

[34] S.V. Ageev, G.O. Iurev, N.E. Podolsky, I.T. Rakipov, L.V. Vasina, B.A. Noskov, A. V. Akentiev, N.A. Charykov, I.V. Murin, K.N. Semenov, Density, speed of sound, viscosity, refractive index, surface tension and solubility of $C_{60}[C(COOH)_2]_3$, J. Mol. Liq. 291 (2019) 111256, https://doi.org/10.1016/j.molliq.2019.111256.

[35] F.I.E.S. Frog, R.A. Kotelnikova, G.N. Bogdanov, V.N. Shtolko, R.V.A.A. Kushch, N. E. Fedorova, A.A. Medzhidova, Effect of amino acid derivatives of fullerene C60 on the development of cytomegalovirus infection, Technol. Living Syst. (2003) 42–46.

[36] R.A. Kotel'nikova, I.I. Faingol'd, D.A. Poletaeva, D.V. Mishchenko, V.S. Romanova, V.N. Shtol'ko, G.N. Bogdanov, A.Yu. Rybkin, E.S. Frog, A.V. Smolina, A.A. Kushch, N.E. Fedorova, A.I. Kotel'nikov, Antioxidant properties of water-soluble amino acid derivatives of fullerenes and their role in the inhibition of herpes virus infection, Russ. Chem. Bull. 60 (2011) 1172–1176, https://doi.org/10.1007/s11172-011-0184-x.

[37] S.K. Khalikov, D. Sharipova, S.Z. Zafarov, M. Umarkhon, S.V. Alieva, Synthesis and characterization of fullero-C_{60} α-amino acids with antiviral properties, Chem. Nat. Compd. 53 (2017) 121–127, https://doi.org/10.1007/s10600-017-1924-4.

[38] M. Bjelaković, T. Kop, V. Maslak, D. Milić, Synthesis and characterization of highly ordered self-assembled bioactive fulleropeptides, J. Mater. Sci. 51 (2016) 739–747, https://doi.org/10.1007/s10853-015-9396-z.

[39] Z. Hu, W. Guan, W. Wang, L. Huang, X. Tang, H. Xu, Z. Zhu, X. Xie, H. Xing, Synthesis of amphiphilic amino acid C_{60} derivatives and their protective effect on hydrogen peroxide-induced apoptosis in rat pheochromocytoma cells, Carbon N Y. 46 (2008) 99–109, https://doi.org/10.1016/j.carbon.2007.10.041.

[40] Z. Hu, S. Liu, Y. Wei, E. Tong, F. Cao, W. Guan, Synthesis of glutathione C60 derivative and its protective effect on hydrogen peroxide-induced apoptosis in rat pheochromocytoma cells, Neurosci. Lett. 429 (2007) 81–86, https://doi.org/10.1016/j.neulet.2007.09.063.

[41] Z. Hu, Y. Huang, W. Guan, J. Zhang, F. Wang, L. Zhao, The protective activities of water-soluble C_{60} derivatives against nitric oxide-induced cytotoxicity in rat pheochromocytoma cells, Biomaterials 31 (2010) 8872–8881, https://doi.org/10.1016/j.biomaterials.2010.08.025.

[42] F.-Y. Hsieh, A.V. Zhilenkov, I.I. Voronov, E.A. Khakina, D.V. Mischenko, P. A. Troshin, S. Hsu, Water-soluble fullerene derivatives as brain medicine: surface chemistry determines if they are neuroprotective and antitumor, ACS Appl. Mater. Interfaces 9 (2017) 11482–11492, https://doi.org/10.1021/acsami.7b01077.

[43] Z. Hu, C. Zhang, Y. Huang, S. Sun, W. Guan, Y. Yao, Photodynamic anticancer activities of water-soluble C_{60} derivatives and their biological consequences in a HeLa cell line, Chem. Biol. Interact. 195 (2012) 86–94, https://doi.org/10.1016/j.cbi.2011.11.003.

[44] R.A. Kotel'nikova, D.V. Mishchenko, D.A. Zhokhova, A.V. Barinov, N.S. Goryachev, A.Yu. Rybkin, G.N. Bogdanov, V.N. Varfolomeev, V.S. Romanova, A.I. Kotel'nikov, Luminescent techniques in investigation of the biological properties of fullerene-based hybrid nanostructures, High Energ. Chem. 43 (2009) 582–586, https://doi.org/10.1134/S0018143909070145.

[45] D.M. Darvish, Collagen fibril formation in vitro: from origin to opportunities, Mater. Today Bio. 15 (2022) 100322, https://doi.org/10.1016/j.mtbio.2022.100322.

[46] S. Chattopadhyay, R.T. Raines, Collagen-based biomaterials for wound healing, Biopolymers 101 (2014) 821–833, https://doi.org/10.1002/bip.22486.

[47] M.D. Stein, L.M. Salkin, A.L. Freedman, V. Glushko, Collagen sponge as a topical hemostatic agent in mucogingival surgery, J. Periodontol. 56 (1985) 35–38, https://doi.org/10.1902/jop.1985.56.1.35.

[48] X. Cheng, Z. Shao, C. Li, L. Yu, M.A. Raja, C. Liu, Isolation, characterization and evaluation of collagen from jellyfish rhopilema esculentum kishinouye for use in hemostatic applications, PLoS One 12 (2017) e0169731.

[49] S. Sharma, V.K. Rai, R.K. Narang, T.S. Markandeywar, Collagen-based formulations for wound healing: a literature review, Life Sci. 290 (2022) 120096, https://doi.org/10.1016/j.lfs.2021.120096.

[50] Y.-P. Chen, C.-H. Liang, H.-T. Wu, H.-Y. Pang, C. Chen, G.-H. Wang, L.-P. Chan, Antioxidant and anti-inflammatory capacities of collagen peptides from milkfish (Chanos chanos) scales, J. Food Sci. Technol. 55 (2018) 2310–2317, https://doi.org/10.1007/s13197-018-3148-4.

[51] D. Schwarz, M. Lipoldová, H. Reinecke, Y. Sohrabi, Targeting inflammation with collagen, Clin. Transl. Med. 12 (2022), https://doi.org/10.1002/ctm2.831.

[52] Z. Hu, W. Guan, W. Wang, L. Huang, H. Xing, Z. Zhu, Protective effect of a novel cystine $_{C_6}$0 derivative on hydrogen peroxide-induced apoptosis in rat pheochromocytoma PC12 cells, Chem. Biol. Interact. 167 (2007) 135–144, https://doi.org/10.1016/j.cbi.2007.02.009.

[53] A.O.E. Abdelhalim, V.V. Sharoyko, S.V. Ageev, V.S. Farafonov, D.A. Nerukh, V. N. Postnov, A.V. Petrov, K.N. Semenov, Graphene oxide of extra high oxidation: a wafer for loading guest molecules, J. Phys. Chem. Lett. 12 (2021) 10015–10024, https://doi.org/10.1021/acs.jpclett.1c02766.

[54] N.E. Podolsky, M.I. Lelet, S.V. Ageev, A.V. Petrov, A.S. Mazur, N.R. Iamalova, D. N. Zakusilo, N.A. Charykov, L.V. Vasina, K.N. Semenov, I.V. Murin, Thermodynamic properties of the $C^{70}(OH)^{12}$ fullerenol in the temperature range T = 9.2 K to 304.5 K, J. Chem. Thermodyn. 144 (2020) 106029, https://doi.org/10.1016/j.jct.2019.106029.

[55] D.N. Nikolaev, N.E. Podolsky, M.I. Lelet, N.R. Iamalova, O.S. Shemchuk, S. V. Ageev, A.V. Petrov, K.N. Semenov, N.A. Charykov, L.B. Piotrovskiy, I.V. Murin, Thermodynamic and quantum chemical investigation of the monocarboxylated fullerene $C_{60}CHCOOH$, J. Chem. Thermodyn. 140 (2020), https://doi.org/10.1016/j.jct.2019.105898.

[56] E.I. Pochkaeva, A.A. Meshcheriakov, S.V. Ageev, N.E. Podolsky, A.V. Petrov, N. A. Charykov, L.V. Vasina, O.Y. Nikolaeva, I.N. Gaponenko, V.V. Sharoyko, I. V. Murin, K.N. Semenov, Polythermal density and viscosity, nanoparticle size distribution, binding with human serum albumin and radical scavenging activity of the C_{60}-l-arginine $(C_{60}(C_6H_{13}N_4O_2)_8H_8)$ aqueous solutions, J. Mol. Liq. 297 (2020) 111915, https://doi.org/10.1016/j.molliq.2019.111915.

[57] H. Akbaş, A. Karadağ, A. Aydın, A. Destegül, Z. Kılıç, Synthesis, structural and thermal properties of the hexapyrrolidinocyclotriphosphazenes-based protic molten salts: antiproliferative effects against HT29, HeLa, and C6 cancer cell lines, J. Mol. Liq. 230 (2017) 482–495, https://doi.org/10.1016/j.molliq.2017.01.067.

[58] A.O.E. Abdelhalim, S.V. Ageev, A.V. Petrov, A.A. Meshcheriakov, M.D. Luttsev, L. V. Vasina, I.A. Nashchekina, I.V. Murin, O.E. Molchanov, D.N. Maistrenko, A. A. Potanin, K.N. Semenov, V.V. Sharoyko, Graphene oxide conjugated with doxorubicin: synthesis, bioactivity, and biosafety, J. Mol. Liq. 359 (2022) 119156, https://doi.org/10.1016/j.molliq.2022.119156.

[59] T. Riaz, R. Zeeshan, F. Zarif, K. Ilyas, N. Muhammad, S.Z. Safi, A. Rahim, S.A. A. Rizvi, I.U. Rehman, FTIR analysis of natural and synthetic collagen, Appl. Spectrosc. Rev. 53 (2018) 703–746, https://doi.org/10.1080/05704928.2018.1426595.

[60] H. Saitô, M. Yokoi, A ^{13}C NMR study on collagens in the solid state: hydration/dehydration-induced conformational change of collagen and detection of internal motions, J. Biochem. 111 (1992) 376–382, https://doi.org/10.1093/oxfordjournals.jbchem.a123765.
[61] D. Huster, J. Schiller, K. Arnold, Comparison of collagen dynamics in articular cartilage and isolated fibrils by solid-state NMR spectroscopy, Magn. Reson. Med. 48 (2002) 624–632, https://doi.org/10.1002/mrm.10272.
[62] D. Huster, Chapter 4 Solid-State NMR Studies of Collagen Structure and Dynamics in Isolated Fibrils and in Biological Tissues, Annu. Rep. NMR Spectrosc. 64 (2008) 127–159, https://doi.org/10.1016/S0066-4103(08)00004-5.
[63] M. Dmitrenko, A. Zolotarev, V. Liamin, A. Kuzminova, A. Mazur, K. Semenov, S. Ermakov, A. Penkova, Novel membranes based on hydroxyethyl cellulose/sodium alginate for pervaporation dehydration of isopropanol, Polymers (Basel). 13 (2021) 674, https://doi.org/10.3390/polym13050674.
[64] H. Heidari, A. Shamloo, The effect of rippled graphene sheet roughness on the adhesive characteristics of a collagen–graphene system, Int. J. Adhes. Adhes. 64 (2016) 9–14, https://doi.org/10.1016/j.ijadhadh.2015.10.002.
[65] T. Kuilla, S. Bhadra, D. Yao, N.H. Kim, S. Bose, J.H. Lee, Recent advances in graphene based polymer composites, Prog. Polym. Sci. 35 (2010) 1350–1375, https://doi.org/10.1016/j.progpolymsci.2010.07.005.
[66] M. Sosnowska, M. Kutwin, S. Jaworski, B. Strojny, M. Wierzbicki, J. Szczepaniak, M. Łojkowski, W. Święszkowski, J. Bałaban, A. Chwalibog, E. Sawosz, Mechano-signalling, induced by fullerene C_{60} nanofilms, arrests the cell cycle in the G2/M phase and decreases proliferation of liver cancer cells, Int. J. Nanomedicine 14 (2019) 6197–6215, https://doi.org/10.2147/IJN.S206934.
[67] B.M. Baker, A.M. Handorf, L.C. Ionescu, W.-J. Li, R.L. Mauck, New directions in nanofibrous scaffolds for soft tissue engineering and regeneration, Expert Rev. Med. Devices 6 (2009) 515–532, https://doi.org/10.1586/erd.09.39.
[68] A. Zareidoost, M. Yousefpour, B. Ghasemi, A. Amanzadeh, The relationship of surface roughness and cell response of chemical surface modification of titanium, J. Mater. Sci. Mater. Med. 23 (2012) 1479–1488, https://doi.org/10.1007/S10856-012-4611-9.
[69] A.A. Zolotarev, A.I. Lushin, N.A. Charykov, K.N. Semenov, V.I. Namazbaev, V. A. Keskinov, A.S. Kritchenkov, Impact resistance of cement and gypsum plaster nanomodified by water-soluble fullerenols, Ind. Eng. Chem. Res. 52 (2013) 14583–14591, https://doi.org/10.1021/ie400245c.
[70] X. Yin, L. Zhao, S. Kang, J. Pan, Y. Song, M. Zhang, G. Xing, F. Wang, J. Li, R. Zhou, Y. Zhao, Impacts of fullerene derivatives on regulating the structure and assembly of collagen molecules, Nanoscale 5 (2013) 7341, https://doi.org/10.1039/c3nr01469j.